Int. J. Electrochem. Sci., 13 **(2018)** 6296 – 6309, doi: 10.20964/2018.07.59

International Journal of
ELECTROCHEMICAL
SCIENCE
www.electrochemsci.org

Electrochemical Corrosion Behavior of 15Cr-6Ni-2Mo Stainless Steel with/without Stress under the coexistence of CO_2 and H_2S

Xue Hui Zhao[1,2,*], *YaoRong Feng*[2], *ShaWei Tang*[3], *JianXun Zhang*[1]

[1] School of Materials Science and Engineering, Xi'an Jiaotong University, Xi'an 710049, China
[2] State Laboratory for performance and Structure Safety of Petroleum Tubular Goods and Equipment Materials, CNPC Tubular Goods Research Institute, xi'an 710077, China
[3] School of Materials Science and Engineering, Harbin Institute of Technology, Harbin 150001, China
[*]E-mail: zhaoxuehui@cnpc.com.cn

Received: 6 February 2018 / *Accepted:* 23 March 2018 / *Published:* 5 June 2018

An electrochemical study was performed on 15Cr-6Ni-2Mo stainless steel to evaluate its corrosion behavior. The specimens in the present study were divided into two groups: with and without applied stress. Three conditions were considered and showed significant influence on the corrosion behavior of 15Cr-6Ni-2Mo steel. When the conditions of coexisting CO_2 and H_2S were changed, the passivation state of the material surface had obvious differences. Applied stress decreased the corrosion potential and pitting potential and increased the pitting sensitivity of the materials. The influence of H_2S on the corrosion resistance of materials under stress was more obvious.

Keywords: Stainless Steel, Polarization curves, Stress corrosion, Corrosion Behavior, Pitting potential

1. INTRODUCTION

With the continuously increasing demand for energy and the continuous exploitation of oil-gas fields, downhole tubing corrosion induced by CO_2 is a great threat to integrity of oil-wells, and in most situations, the presence of H_2S and applied stress accelerate corrosion problems [1-4]. Failure accidents caused by corrosion fatigue of an oil well pipe string is a serious environmental threat and also causes great economic loss [5-7]. Thus, the combination of the harsh corrosive environment of an oil well pipe string and the current energy shortage make it is necessary to study and develop more scientific, reasonable, and effective corrosion protection methods [8-10]. However, in terms of economic cost, corrosion resistance, long-term maintenance costs, and service life, each protection method has its advantages and disadvantages. Using a corrosion resistant alloy has proved to be a feasible way to solve the corrosion problem because of its relatively low cost and excellent properties

[11-12]. Various corrosion resistant alloys, including low Cr alloy, 13Cr, 22Cr, and nickel-based alloys, have been developed as downhole tubing in different oil field environments [13-19]. However, oil field environments are complicated and distinct, and this limits widespread use of corrosion resistant alloys. At the same time, adaptability between oil field environments and materials is currently a serious problem. In other words, high level material will be overqualified, and low level material will be invalid [20-24]. 15Cr-6Ni-2Mo stainless steel alloy is a new type of martensitic stainless steel that was recently developed in response to the demands of high pressure high temperature oil wells [16]. To date, there have been few works reported on the study of the corrosion behavior of 15Cr-6Ni-2Mo when CO_2 and H_2S were added under different conditions. Meanwhile, there have not been many reports about the corrosion behavior of 15Cr-6Ni-2Mo under stress in an environment of H_2S and CO_2 in the presence of Cl^-. In an oil field environment, CO_2 and H_2S are very aggressive toward the oil well pipe string. In general, CO_2 dissolved in electrolyte can remain in equilibrium with water, and this can be described using equations (1-3) [4，25-26]:

$$CO_2 + H_2O \leftrightarrow H_2CO_3 \quad (1)$$

$$H_2CO_3 \leftrightarrow H^+ + HCO_3^- \quad (2)$$

$$HCO_3^- \leftrightarrow H^+ + CO_3^{2-} \quad (3)$$

H_2S gas can dissolve in water and work as a cathodic depolarizer; this can be expressed using equations (4-7) [17-18]:

$$H_2S \leftrightarrow H_2S_{ad} \quad (4)$$

$$H_2S_{ad} + e \rightarrow H_{ad} + HS_{ad}^- \quad (5)$$

$$HS_{ad}^- + H^+ \rightarrow H_2S \quad (6)$$

$$H_{ad} + H_{ad} \rightarrow H_2 \quad (7)$$

This paper aims to investigate the electrochemical behavior of 15Cr-6Ni-2Mo with and without stress under coexisting CO_2 and H_2S. Using a combination of potentiodynamic polarization and electrochemical impedance spectroscopy (EIS), the electrochemical behavior of 15Cr-6Ni-2Mo was investigated, and the effects of H_2S and applied stress were evaluated. It is anticipated that this paper can provide insight into the passive film behavior in different test conditions and clarify the relationship between its electrochemical behavior and passivation characteristics.

2. EXPERIMENTAL

2.1. Materials and solutions

Experimental material was selected from high strength 15Cr-6Ni-2Mo stainless steel tubing; according to the manufacturer, the chemical composition (wt%) was: C 0.024, S 0.002, N 0.02, P 0.013, Si 0.28, Cr 15.22, Ni 6.31, Mn 0.18, Mo 2.11, Cu 0.41, and Fe balance. The metallurgic structure of the specimens was tempered martensite (Fig.1).

The specimens in the present study were divided into two groups: those with and those without applied stress. Rectangular specimens for the electrochemical corrosion test were 57 mm×10 mm×3 mm (width×length×thickness). Before each experiment, all of the specimens were polished with 2000

grit SiC paper to obtain a smooth specimen surface and to minimize errors caused by surface roughness. Finally, the specimens were cleaned with distilled water and ethanol, dried with cool air, and stored in a dry N_2 atmosphere.

Three test conditions were considered in the present study. The first was a saturated CO_2 solution (named as Test 1). In the second condition, H_2S was introduced into the saturated CO_2 solution when the open circuit potential (OCP) was stable (named as Test 2). In the third condition, H_2S and CO_2 were simultaneously introduced into the base solution (named as Test 3). The test solution, which simulated the formation water in an oil field, was made from analytical grade reagents and deionized water, and the Cl^- concentration was 20g/L. An oil bath was used to maintain the temperature of the test solutions. In this test, a certain amount of $Na_2S{\cdot}9H_2O$ (0.05 g/ L) was added to the test solution instead of H_2S.

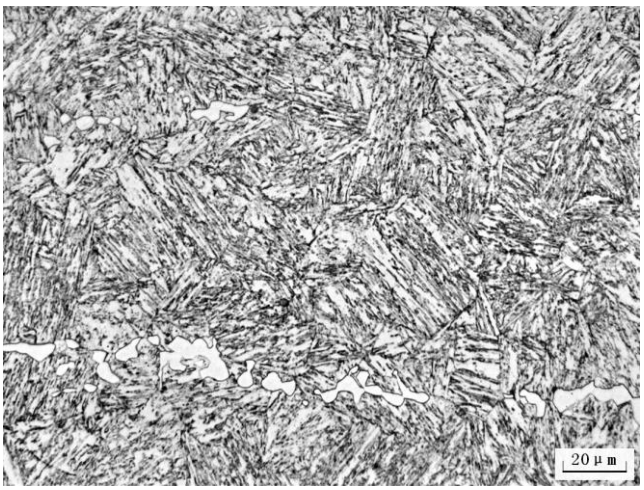

Figure 1. Microstructure of materials.

2.2. Electrochemical tests

Electrochemical measurements were carred out using an electrochemical system with a typical three-electrode electrochemical cell. The working electrode was a rectangular specimen, the counter electrode was two parallel graphite rods, and the reference electrode was silver chloride (Ag/AgCl) with saturated potassium chloride (KCl) solution.

The potentiodynamic polarization curves were recorded over a potential range from -200 mV to 800 mV versus OCP with a scan rate of 0.3 mV/s. From the polarization curves, OCP, corrosion potential (E_{corr}), passivation current density (I_p), and pitting potential (E_{pit}) were obtained. E_{ocp} is the potential between the working electrode and reference electrode when no electrical current flows. I_p is the passivation current density at which steel is in a stable passive state. E_{pit} is the potential when the corrosion passive film breaks down and leads to a rapid increase in the current density.

A four point bending method was used to load the stress. A diagram of the applied stress is shown in Fig. 2(a); the space between the specimen and clamp was insulated by four white Teflon round bars. Electrochemical specimens were welded to a copper wire as the working electrode joint, and the weld points were sealed with epoxy to prevent galvanic corrosion between dissimilar metals.

The yield strength (σ_s) of the experimental material at room temperature was 825 MPa, which was provided by the manufacturer, and for experiments, the loading stresses of the specimens were 0% σs (no-stress test), 70% σs, 80% σs, and 90% σs.

Also, to reduce the experimental error and to ensure the reproducibility of the experiment, the stress concentration area (region A) of the specimen was exposed to the solution (the exposed area was 2.8 $cm^{2)}$, and the rest of the area was sealed with a high temperature resistant epoxy resin (Fig.2(b)). In these tests, the specimen surface was ground to a smooth finish of $R_a \leq 0.2\mu m$. *y* is just below the proportional limit of the load-strain curve, from which a known elastic stress (σ) can be calculated using the following equation [19]:

$$\sigma = \frac{12Ety}{\left(3H^2 - 4A^2\right)} \tag{7}$$

where *E* is the elastic modulus, *A* and *H* are the distances between the inner and outer supports respectively, and *t* is the specimen thickness.

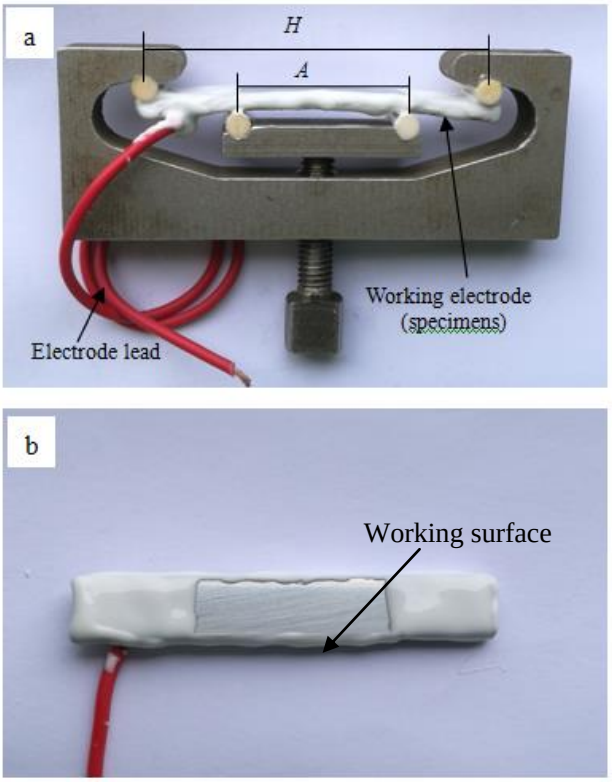

Figure 2. (a) Diagram of applied stress and specimens; (b) specimen.

EIS measurements were performed at OCP using an alternating current voltage amplitude of 0.005 V. The frequency was varied from 0.01 to 100,000 Hz, and the AC voltage amplitude was 10 mV.

All of the tests were carried out in a circulating oil bath, and a temperature monitoring system was used to control the temperature. All of the curves were tested at least three times to ensure the stability and reproducibility of the tests.

3. RESULTS AND DISCUSSION

3.1. OCP measurement

Under the conditions of the CO_2-saturated environment and with added H_2S gas, the pH of the solution system changed obviously with dissolution of the corrosive gas. This change in pH affected the interfacial reaction mechanism of the material and the media, affected electron transfer between the surface of the specimen and the media, and affected formation of the corrosion product film [27-29].Therefore, when H_2S was added under different test conditions, the corrosion potential of the specimen showed different trends with the dissolution of CO_2/H_2S and with the interfacial reaction.

Time evolution of the OCP for the 15Cr-6Ni-2Mo specimens without stress in three experimental conditions is presented in Fig. 3. Comparison of the test results shows that the obtained OCP values for Test 1 were always more positive, and this indicates that the surface passivation of the specimen was better in the saturated CO_2 environment and that a stable potential was gradually achieved. A more negative potential for the specimens in Test 2 indicate that added H_2S affected the stability of the corrosion film that formed in the early stage.

The OCP of specimens in Test 3 is relatively lower at the beginning, and this indicates that the specimens were more sensitive to corrosion in the environment with coexisting H_2S and CO_2. The potential increased over time, and this shows that the combination of H_2S+CO_2 influenced the kinetics of the anodic reaction and had a significant effect on the passivation of the specimen surface. This difference can be related to the added H_2S. Finally, with formation of the corrosion film, the OCP of the specimens increased gradually and tended to be stable.

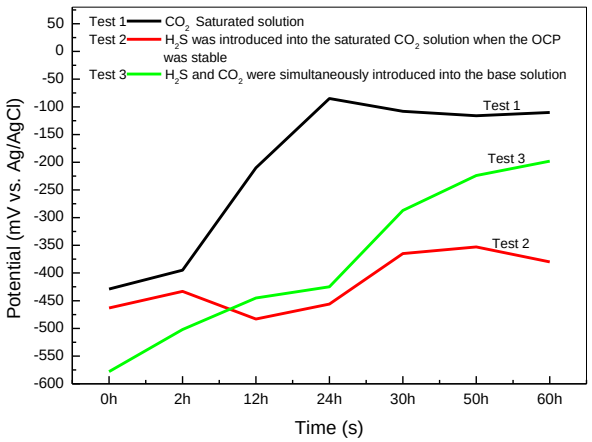

Figure 3. Changes in the open-circuit potential over time for specimens without stress in different test conditions.

3.2. Potentiodynamic polarization behavior

3.2.1. Polarization curves of specimens without stress

Fig. 4 shows the potentiodynamic polarization curves of specimens without stress in the three experimental conditions. A distinct active-passive transition of each specimen was observed in the

studied potential range [12]. Nonetheless, there were obvious discrepancies between the polarization behaviors of the different experimental conditions, and the corrosion potential in Test 1 was more positive. When H_2S was added to the experimental solution, the corrosion potential decreased, and the corrosion potential in Test 3 was the most negative. Table 1 lists some of the corresponding electrochemical parameters.

Plateaus of current densities present in curves 1 and 3 indicate distinct passivation-like behavior over a wide range of anodic potentials; the anodic dissolution area was relatively small, and E_{pp} was achieved after a short time. This behavior revealed that the specimen had remarkable passivation behavior under the test conditions, and the passivation film hindered further corrosion of the materials. The value of I_p was relatively stable, and this indicates that the passivation film was dense and completely hindered electron transfer between the material and medium. Thus, when the anodic potential was increased, the corrosion current density remained unchanged. The values of I_p for Tests 1 and 3 were about 8.9×10^{-6} A cm^{-2} and 9.4×10^{-6} A cm^{-2}, respectively. According to the I_p values, the corrosivity of Test solution 1 was relatively small.

Curve 3 is the polarization curve for the combined environment of H_2S and CO_2, and the reaction mechanism was quite different from that of the other condition (curve 1). Absorptivity of HS^- is stronger in acidic solution, and HS^- was prone to adsorb and discharge on the iron electrode. A layer of Fe_xS_y, which was derived from the stoichiometric ratio of ferrous sulfide, was deposited on the surface of the electrode. S^{2-} can form a coordination bond with Fe or Fe^{2+} because of its strong discharging ability. Adhesion of the corrosion product film was improved. As the reaction proceeds, the concentration of S^{2-} decreases, excess Fe^{2+} reacts with CO_3^{2-} and HCO_3^-, and a large amount of carbonate is produced [30-31]. Formation of carbonate was slow, and the size of the product was relatively small. Thus, carbonate filled the pores of the sulfide product, and the surface film became more compact. This film can effectively block electron transfer, and a surface passivation state was obtained.

However, an unstable anodic passivation region was observed for Test 2, and this indicates that there is a dynamic equilibrium reaction between the rupture and self-healing of the passive film. At the beginning of the experiment, the specimens reacted with the CO_2-saturated solution. A carbide corrosion product formed rapidly on the surface of the specimen (equations (9-12)). When $Na_2S\cdot9H_2O$ was added to the CO_2-saturated solution, hydrogen sulfide formed rapidly and was involved in the polarization reaction; dissolution of carbide and the formation of new mixed corrosion products formed a complex dynamic equilibrium reaction. Thus, when the anodic current density was increased slightly with an increase in potential, this demonstrated that formation of the passive film only inhibited the corrosion process, whereas local corrosion could not be avoided because of the presence of an electron transport channel in the passive film. When the anodic potential reached -172mV, the new mixed products became stronger; the anodic current density then decreased gradually, and the surface of the specimen was in a passive state. The passivation current density (I_p) was 8.5×10^{-5}A/cm^2. When the anodic potential reached the critical breakdown potential (E_{pit}), the anodic current density increased immediately.

$$CO_2 + H_2O \rightarrow H_2CO_3 \quad (9)$$

$$H_2CO_3 + e^- \rightarrow H^+ + HCO_3^- \quad (10)$$

$$H + H \rightarrow H_2 \uparrow \quad (11)$$

$$Fe + H_2CO_3 \rightarrow FeCO_3 + H_2 \quad (12)$$

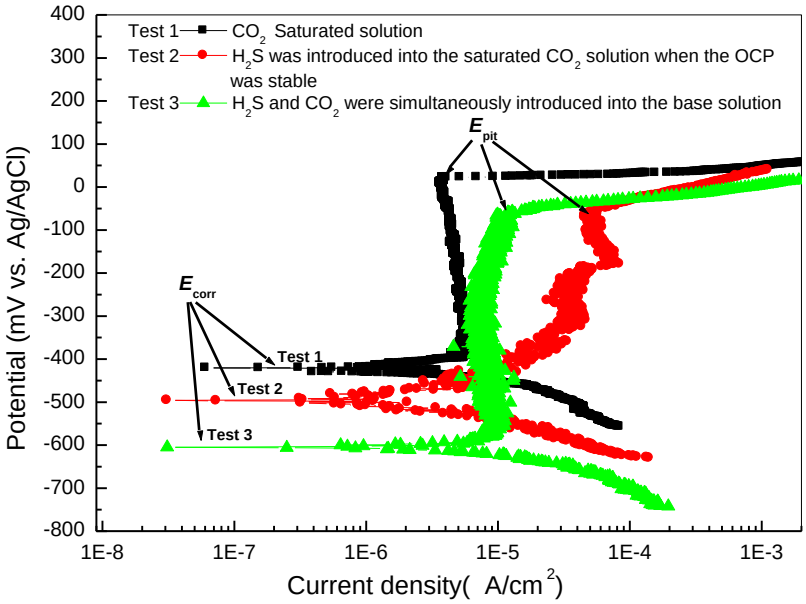

Figure 4. Potentiodynamic polarization curves of specimens in different CO_2/H_2S conditions.

Table 1. Corresponding electrochemical parameters of polarization curves

Conditions	E_{corr} (mV)	I_{corr} (A/cm^2)	E_{pit} (mV)	I_p (A/cm^2)
Test 1	-421	7.5E-7	15.7	8.9E-6
Test 2	-496	8.9E-7	-45	8.5E-5
Test 3	-605	3.2E-6	-64	9.4E-6

3.2.2 Effects of loading stress on polarization curves

Not much has been reported on the study of corrosion properties of 15Cr-6Ni-2Mo stainless steel under stress. Under the conditions of high temperature and high pressure CO_2, Zhao et al. [32] studied the effects of different H_2S partial pressures on pitting sensitivity and stress cracking sensitivity of 15Cr-6Ni-2Mo stainless steel at 150℃. Lv et al. [33] studied the effects of an acidic environment and corrosion inhibitor on corrosion potential and corrosion morphology of 15Cr stainless materials at 170℃. Results showed that a high concentration of H_2S decreased the pitting potential and increased the cracking sensitivity of the material, and the corrosion inhibitor effectively improved the corrosion resistance of the material. However, the electrochemical performance of 15Cr-6Ni-2Mo under stress was not further studied.

To study the corrosion performance of the materials under stress, electrochemical corrosion behaviors of the materials under different applied stress conditions were simulated. The corrosion

media were saturated CO_2 and the conditions of coexisting H_2S+CO_2. The concentration of Cl^- was 20 g/L. The experimental temperature was controlled at 90℃.

Corrosion performances of specimens under the combined conditions of stress and corrosion media are shown in Figs. 5 and 6. Table 2 lists some of the corresponding electrochemical parameters.

As seen in Fig. 5, under the stress and test temperature conditions, the values of E_{corr} are -458 mV, -500 mV, and -475 mV. The values of E_{corr} for specimens under applied stress are lower than those for specimens under no stress (-416 mV). As observed, with an increase in applied stress, the corrosion potential decreased, and the anode passivation region became increasingly unstable; this indicates that the applied stress enhanced surface activity. The specimen surface remained in a state of dynamic balance between microcorrosion and self-repair.

When the applied stress is greater than or equal to 80%σ_s, the anodic curve shifted to the right, and the anodic current density obviously increased; this suggests that the corrosion resistance decreased under greater stress. In contrast with the other curves, there is no stable passivation zone in curve 3, and this indicates that the passive film on the specimen surface was not completely formed and that there is still an electron transfer channel between the solution medium and the material, enabling corrosion to continue to occur. Curves 3 and 4 show a similar value of E_{pit} (about -22 mV), which is lower than that of the specimens without stress or with lower stress (curves 1 and 2), and this suggests that stress enhanced the pitting susceptibility of materials. When the surface potential reached E_{pit}, the active surface film layer broke down, the corrosion current increased rapidly, and the pitting phenomenon occurred.

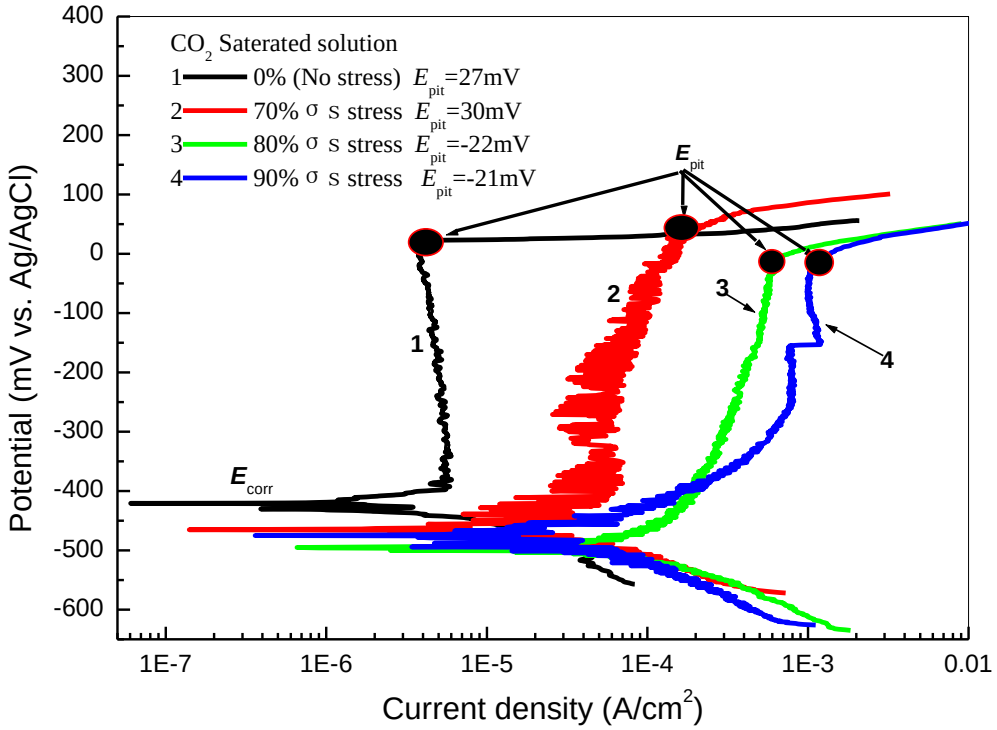

Figure 5. Potentiodynamic polarization curves of specimens with and without stress in the CO_2 saturated solution system.

Table 2. Corresponding electrochemical parameters of polarization curves in CO_2-saturated solution

Applied stress （MPa）	E_{corr} (mV)	I_{corr} (A/cm^2)	E_{pit} (mV)	I_p (A/cm^2)
0%σ_s (no-stress)	-416	7.5E-7	27	4.5E-6
70% σ_s	-458	5.2E-6	30	5.8E-5
80% σ_s	-500	7.8E-6	-22	/
90% σ_s	-475	9.5E-6	-21	7.5E-4

Polarization curves of specimens with and without applied stress in the combined H_2S+CO_2 condition were obtained (Fig. 6). The values of applied stress were 80%σ_s and 90%σ_s, and the test temperature was 90℃. The corrosion potential of specimens under applied stress decreased from -594 mV to -672 mV with an increase in the applied stress. At the same time, the polarization curve moved to the right, which indicates that the applied stress also promoted an increase in the corrosion rate.

Compared with the results of the CO_2-saturated condition, the values of E_{corr} for specimens in H_2S+CO_2 conditions all decreased. From thermodynamics analysis, materials are more susceptible to corrosion in the conditions with the combined H_2S+CO_2. In acidic conditions containing H_2S, the cathode reaction was strengthened because of adsorption of H^+ and depolarization effects on the surface; also, the anodic active reaction was accelerated. Moreover, the corrosion medium of H_2S is one of the main factors that lead to stress corrosion cracking.

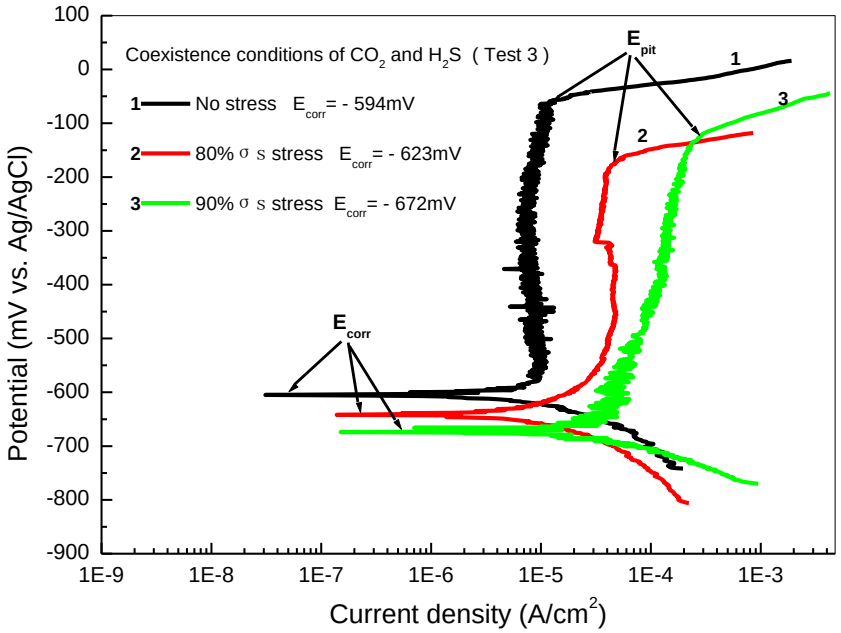

Figure 6. Potentiodynamic polarization curves of specimens under stress and not under stress in the presence of CO_2 and H_2S.

Fig.7 shows the microscopic morphologies of the surface of each specimen after testing the polarization curves. A small amount of pits are found on the surface of the specimens without applied

stress (Fig.7 (a)), whereas the specimens loaded with 80%σs and 90%σs have a large number of tiny pits that are evenly distributed on the surface of the specimens. With an increase in the loading stress, the degree of pitting corrosion increased, and this indicates that stress makes the surface of the material become a relatively high active state and improves the pitting sensitivity.

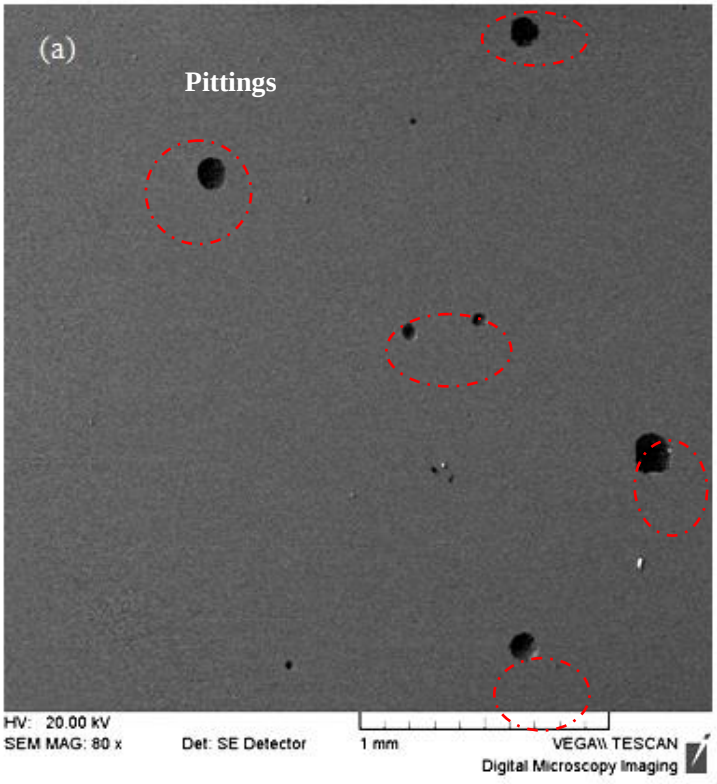

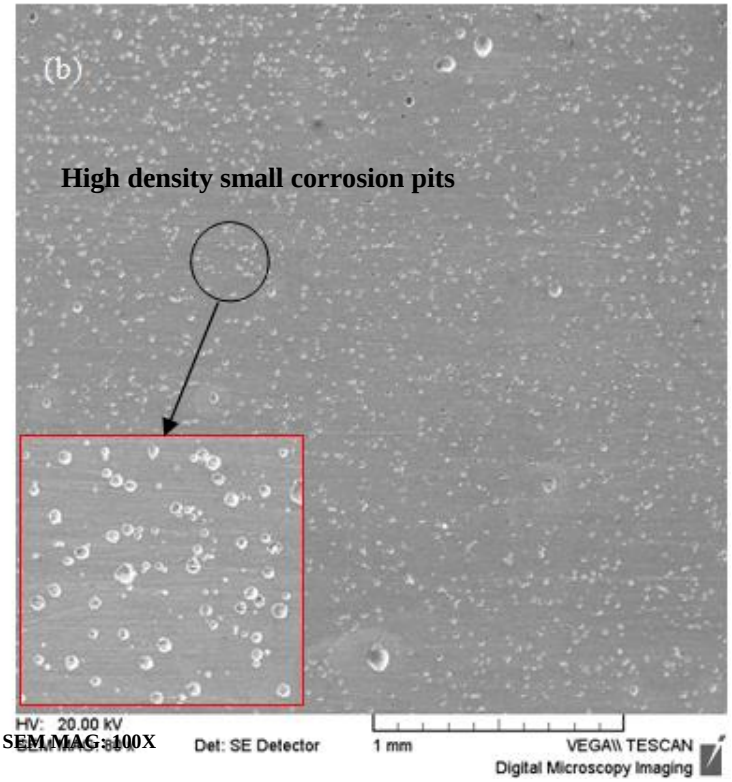

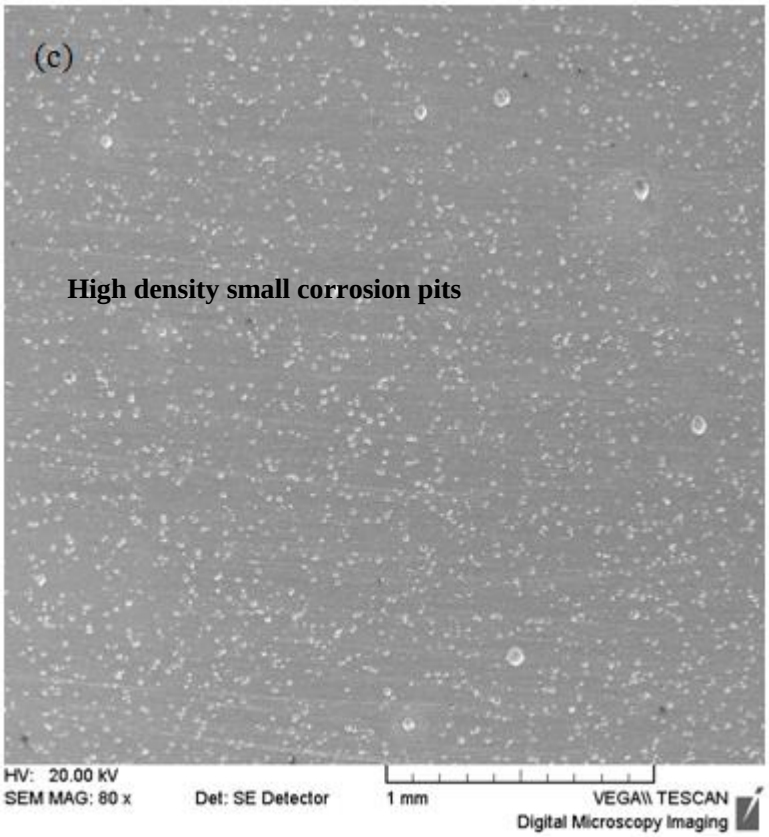

Figure 7. SEM surface morphologies of the specimens after testing polarization curves：(a) no stress, (b) 80%σ_s stress, and (c) 90%σ_s stress.

During potentiodynamic anodic polarization, an increase in the anodic polarization potential caused the passive film on the surface to begin to crack when the potential reached the critical breaking potential. The polarization current increased rapidly, and pitting occurred at this point [34]. In contrast to Fig. 6, curve 1 in Fig. 7 (a) shows that when the polarization potential of the specimen reached E_{pit}, pitting corrosion occurred on the surface of the specimen. When the specimen was loaded with stress, the tensile stress increased the surface activity of the material and accelerated adsorption of Cl^- and OH^- on the surface of the material. Moreover, with an increase in stress, the adsorption rate of Cl^- was accelerated, and the the amount of adsorbed Cl^- increased [35-36].

This is consistent with the results of curves 2 and 3 in Fig. 6. The corrosion current density is relatively larger, and there is no obvious stable passivation region. Curves 2 and 3 also show that the critical breaking potential of the material is relatively lower and that with an increase in the anodic polarization potential, the passivation film was quickly broken down and high density corrosion pits appeared.

3.3. Electrochemical impedance spectroscopy

EIS was measured at the OCP for the specimens both with/without applied stress in different test solutions. The obtained impedance Nyquist spectra are presented in Fig.8. The specimens all have

similar impedance features; the impedance arc has a single incomplete half arc under the condition of no stress, and the radius is relatively larger than that of under stress. When the specimens were loaded with different stress (0, 80%σ_s, and 90%σ_s), the impedance radius decreased with an increase in the stress value. This indicates that applied stress affects the activity of the specimen surface, the speed of electron exchange at the metal/solution medium interface is promoted, and corrosion is accelerated. In the combined environment of H_2S+CO_2, the changing amplitude of the impedance arc radius is relatively larger for the stressed state; this indicates that surface corrosion of the material is more sensitive in an H_2S environment, film protection is poor, and charge transfer resistance is relatively small. These observations from the impedance spectra are consistent with the results obtained from the polarization curves.

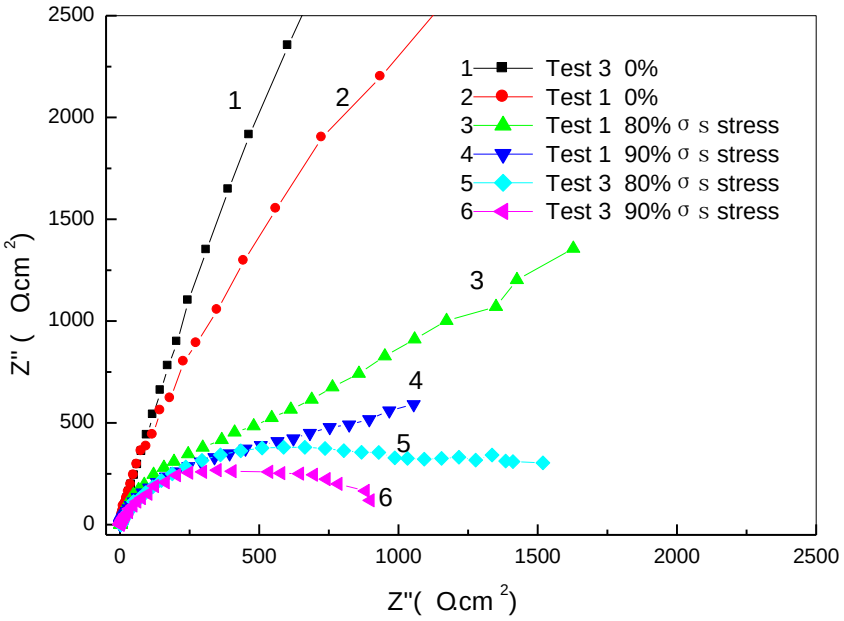

Figure 8. Electrochemical impedance spectra of the specimens with/without applied stress in saturated CO_2 and H_2S+CO_2 conditions.

4. CONCLUSIONS

The corrosion behavior of 15Cr-6Ni-2Mo tubing was studied using electrochemistry at 90℃, and the effects of CO_2/H_2S and tensile stress on corrosion behavior were evaluated.

(1) Under the conditions of CO_2-saturated solution and solution of coexisting CO_2+H_2S, the specimens without stress quickly reached a passive state, the passivation zone was relatively wider, and the passivation current density was stable. Although the anodic dissolution zone was relatively wider under the conditions of Test 2, the passivation phenomenon appeared slowly, and passivation current density was relatively larger.

(2) Under the condition of CO_2-saturated solution, with an increase in the applied stress, the passivation state of the material surface was rather unstable. Pitting corrosion potential decreased

gradually, but the corrosion potential of the material did not change significantly for states with different amounts of stress.

(3) For the combination of CO_2+H_2S, the corrosion potential and pitting potential decreased with an increase in the applied stress. The polarization curve gradually shifted to the right, and the passive current density increased. Micro-corrosion morphology shows that stress increased the surface activity of the materials and improved the pitting sensitivity of the materials.

(4) The impedance spectrum results show that the impedance radius of the material decreased obviously under stress. Also, the influence of H_2S on the corrosion resistance of the material was more obvious.

ACKNOWLEDGEMENTS

This research was funded by the China National Petroleum Corporation for Science Research and technology development project (2017D-2307), and the Shaan xi Province Nature Science Foundation of China under Contracts of 2012JQ6014.

References

1. Shao.Q. Guo, L.N. Xu, L. Zhang, W. Chang, M.X. Lu, *Corros. Sci*., 110 (2016) 123.
2. Y. Xiang, C. Li, Z.W. Long, C.Y. Guan, W.Wang, W. Hesitao, *Electrochim. Acta*, 258 (2017) 909.
3. G. Hinds, L. Wickström, K. Mingard, A. Turnbull, *Corros. Sci.*, 71 (2013) 43.
4. G.A. Zhang, Y. Zeng, X.P. Guo, F. Jiang, D.Y. Shi, Z.Y. Chen, *Corros. Sci.*, 65 (2012) 37.
5. Y.S. Choi, S. Nesic, S. Ling, *Electrochim. Acta*, 56 (2011) 1752.
6. A.H.S. Bueno, E.D. Moreir, J.A.C.P. Gomes, *Appl. Surf. Sci*., 36 (2014) 423
7. Y. Liu, L.N. Xu, M.X. Lu, Y. Meng, J.Y. Zhu, L. Zhang, *Appl. Surf. Sci.*, 30 (2014) 768.
8. Digby D. Macdonald, Adan Sun, *Electrochim. Acta*, 8 (2006) 1767.
9. J.Y. Dai, G.Q. Tang, *Shandong Chemical Industry*, 43 (2014) 58-60.
10. L. Yang, M.M. Hou, *Total Corrosion Control*, 28 (2014) 26.
11. S. Ningshen, M. Sakairi, K. Suzuki, S. Ukai, *Corros. Sci*., 78 (2014) 322.
12. E. Oguzie, J.B. Li, Y.Q. Liu, D.M. Chen, Y. Li, K. Yang, F.H. Wang, *Electrochim. Acta*, 55 (2010) 5028.
13. B.S. Wang, K.J. Luo, M.C. Zhang, J.X. Dong, *The World Steel*, 5 (2009) 42.
14. Q.L. Wu, Z.H. Zhang, X.M. Dong, J.Q.Yang, *Corros. Sci*., 75 (2013) 400.
15. Thiago J. Mesquita, E. Chauveau, M. Mantel, N. Bouvier, D. Koschl, *Corros. Sci*., 81 (2014) 152.
16. T.J. Mesquita, E. Chauveau, M. Mantel, NKRP. Nogueira, *Mater.Chem. Phys.*, 132 (2012) 967.
17. A. Pardo, M.C. Merino, A.E. Coy, F. Viejo, R. Arrabal, E. Matykina, *Corros. Sci*., 50 (2008) 1796.
18. Y. Xie, Y.Q. Wu, J. Burns, J.S. Zhang, *Mater. Charact.*, 112(2016) 87.
19. J.Q. Wan, Q.X. Ran, J. Li, Y.L. Xu, X.S. Xiao, H.F. Yu, L.Z. Jiang, *Materials & Design*, 53 (2014) 43.
20. S.L. Lv, W.W. Song, X.T. Yang, J.X. Peng, Y. Han, G.X. Zhao, X.H. Lv, Z.D. Guo, Y.X.Wen, *Corrosion & Protection*, 36（2015）76.
21. S. Fajardo, D.M. Bastidas, M. Criado, J.M . Bastidas, *Electrochim. Acta*,129 (2014) 160.
22. S.D. Zhu, J.F. Wei, R. Cai, Z.Q. Bai, G.S. Zhao, *Eng. Fail. Anal.*,18 (2011) 2222.
23. R. Ebara, *Procedia Engineering*, 2 (2010) 1297.
24. S.G. Acharyya , A. Khandelwal, V. Kain, A. Kumar, I. Samajdar. *Mater. Charact.*, 72 (2012) 68

25. Y.G. Zheng, B. Brown, S. Nesic. *Corrosion (Houston, TX, U. S.)* ,70 (2014) 351.
26. *L.L. Machuca, S.I. Bailey, R. Gubner. Corros. Sci.*, 64 (2012) 8-16.
27. X.W. Lei, Y.R. Feng, J.X. Zhang, A.Q. Fu, C.X.Yin, D. Macdonald, *Electrochim. Acta*, 10 (2016) 640.
28. Y. Choi, S. Nesic, S. Ling, *Electrochim. Acta*, 56 (2011) 1752.
29. C. Plennevaux, J. Kittel, M. Frégonèse, B. Normand, F. Ropital, F. Grosjean, T. Cassagne, *Electrochem. Commun.*, 26 (2013) 17.
30. G. Verri, K. S. Sorbie, M. A. Singleton, C. Hinrichsen, Q. Wang, F. F. Chang, S. Ramachandran, *SPE International Oilfield Scale Conference and Exhibition, Aberdeen, Scotland, UK*, 2016
31. H. Takabe，K. Kondo, H. Amaya, T. Ohe, Y. Otome, S. Nakatsuka, M. Ueda, *CORROSION 2012, ake City, Utah*, 2012
32. X.H. Zhao, Y.R. Feng, C.X. Yin, Y. Han, *Corros. Sci. Prot. Technol.*, 28(2016)326
33. X.H. Lv, F.X. Zhang, X.T. Yang, J.F. Xie, G.X. Zhao, Y. Xue, *J. Iron.Steel. Res. Int*., 21 (2014) 774
34. Y. Sun, J. Hu . Metal Corrosion and Control. Harbin: *Harbin Institute of Technology Press*, 2003.
35. C.M. Xu, Y.H. Zhang, G.X. Cheng, W.S. Zhu, *Mater. Charact*., 59(2008) 245.
36. J.H. Ding, L. Zhang, M.X. Lu, J. Zhang, Z.B.Wen, W.H. Hao. *Appl. Surf. Sci*., 15 (2014) 33.